Electron affinity of uranium and bound states of opposite parity in its anion

Rulin Tang,[1] Yuzhu Lu ☉,[1] Hongtao Liu,[2,*] and Chuangang Ning ☉[1,3,†]

[1]*Department of Physics, State Key Laboratory of Low-Dimensional Quantum Physics, Tsinghua University, Beijing 100084, China*
[2]*Key Laboratory of Interfacial Physics and Technology, Shanghai Institute of Applied Physics, Chinese Academy of Sciences,*
Shanghai 201800, China
[3]*Collaborative Innovation Center of Quantum Matter, Beijing 100084, China*

The electronic structures of actinide systems are extremely complicated because of strong electron correlations and relativistic effects. The atomic actinide anion poses even more challenges for experimental and theoretical investigations due to the extra loosely bound electron. In this work, we report the electronic structure of U^- using the slow-electron velocity-map imaging method. The electron affinity of U was measured to be 314.97(9) meV. Two excited states of U^- were observed and their energies were determined to be 84(11) and 160(12) meV above its ground state, respectively. The present study provides convincing evidence that the transition between the first excited state and the ground state of U^- is electric dipole ($E1$) allowed.

Studies of simple actinide compounds' physical and chemical properties are of interest from both practical and scientific perspectives. From the practical view, the knowledge of actinides is of great importance for the nuclear industry and environmental science. The radioactive waste and spent nuclear materials pose significant technological problems for their safe treatment and long-term storage. Since experiments of radioactive actinide species are expensive and hazardous, the development of theoretical models that can make reliable predictions for the properties of actinide species is keenly required [1–5]. This task is very challenging because of the strong electron correlation and relativistic effects of the partially occupied $5f$ subshell and $6d$ subshell. From the perspective of fundamental scientific significance, the benchmarked data of a simple actinide system can help us to develop relativistic quantum computational models. For actinides, the inner electrons move at significant fractions of the speed of light. The strong relativistic effects profoundly modified energetics and the spatial extent of the atomic orbitals. As a result, sophisticated relativistic computational methods with QED corrections are required [6–9]. Simple diatomic molecules containing a heavy atom are also useful for experiments designed to test the standard model of particle physics. For example, ThO and ThF^+ are candidates for investigations of the electron electric dipole moment (eEDM) [10]. High-precision optical experiments have demonstrated parity violation in heavy atoms [11]. The studies of actinides are also a crucial step towards the chemistry and physics of superheavy elements ($Z \geqslant 104$) [9,12–14].

In the present work, we report the high-resolution photoelectron spectra of atomic uranium anion U^- using the slow-electron velocity-map imaging (SEVI) method [15–17].

The SEVI method features high energy resolution, typically a few cm^{-1} near the photodetachment threshold [18]. Using this method, we have successfully measured electron affinity (EA) values of several transitional and lanthanide elements with accuracy $\sim 1\,cm^{-1}$ [19–25]. Electron affinity measures the capability of an atom to form the corresponding negative ion. It is defined as the energy difference between the ground state of the neutral atom and the ground state of the corresponding anion. Like the ionization potential (IP), EA is a fundamental parameter for understanding chemical reactions [7,26,27]. In this work, we report the measurement of the EA value of the uranium atom. In 1997, Nadeau *et al.* established a lower limit of EA(U) $\geqslant 0.05\,eV$ based on accelerator mass spectrometry (AMS) [28]. There is no spectroscopic measurement of EA(U) so far due to the experimental challenges. Uranium is the heaviest stable element ($Z = 92$). It plays a key role in the nuclear industry and nuclear weapons [29]. A uranium atom has three $5f$, one $6d$, and two $7s$ valance electrons, making U one of the most challenging elements for theoretical calculations. The high-level calculations using the relativistic configuration-interaction (RCI) method by Beck's group predicted that the extra electron could be put into its $6d$ subshell or $7p$ subshell to form bound states of U^- [30]. The two different configurations have opposite parity, making the electric dipole ($E1$) transition possible. A fast $E1$ transition is a prerequisite for laser cooling of negative ions. Over the past few decades, many attempts have been made to find a negative atomic ion with opposite-parity bound states. So far, $E1$ transitions between bound states have been previously observed for only four atomic ions: Os^- [31–35], La^- [35–38], Ce^- [39,40], and Th^- [21,30,41]. Our recent work has shown that Th^- is an excellent candidate for laser cooling of negative ions [21,41]. Using the RCI method, Beck and co-workers predicted the EA value of U to be 175 meV in 1995 [42] and updated it to 373 meV in 2009 [30]. Their work suggested two bound excited states,
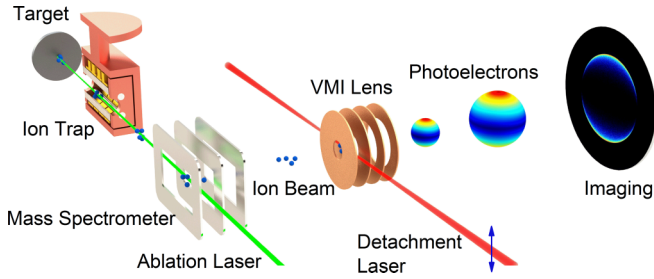
FIG. 1. Schematic view of our cryo-SEVI apparatus. The mass gate and the ion detector before the VMI lens are not shown.

$5f^36d^27s^2\ {}^6M^o_{13/2}$ and $5f^36d7s^27p\ {}^6L^e_{11/2}$, above the ground state $5f^36d7s^27p\ {}^6M^e_{13/2}$. The superscripts o and e indicate the odd and even parity, respectively. Therefore, it is worthwhile to experimentally check whether U− has bound states of opposite parity.

This experiment was carried out on our cryo-SEVI apparatus featuring the combination of the SEVI technique and the cryogenically controlled ion trap [15,16]. Details of the setup have been described previously [17]. A brief introduction is given here. Figure 1 shows the schematic diagram of the experimental apparatus. Negative ions were generated by focusing a 532-nm Nd: YAG pulsed laser onto a metal target. The negative ions were then accumulated and confined in an octupole radio-frequency (rf) ion trap, where they thermally equilibrated with a burst of cold buffer gas by sufficient collisions in 3–45 ms. The typical buffer gas was a mixture of 20% H_2 and 80% He [43]. The ion trap was mounted on the second stage of a liquid helium refrigerator with a variable temperature 5–300 K. The trapped ions could be ejected out via pulsed potentials and were analyzed by a Wiley-McLaren type time-of-flight (TOF) mass spectrometer [44]. Ions of interest were selected via a mass gate and then photodetached by a tunable laser in the interaction zone of the velocity-map imaging (VMI) system [45]. Outgoing electrons formed a spherical shell and were projected onto a phosphor screen behind a set of microchannel plates. The electron hitting positions were recorded in an event-count mode via a charge-coupled device camera and accumulated for typically 50 000 laser shots. The apparatus ran at a 20-Hz repetition rate. The photodetachment laser had a linear polarization parallel to the phosphor screen. Since the distribution of outgoing photoelectrons had a cylindrical symmetry about the polarization axis, the photoelectron distribution could be reconstructed from the projected imaging via the maximum entropy velocity Legendre reconstruction (MEVELER) method [46]. The binding energy of the transition was extracted by $BE = h\nu - ar^2$, where $h\nu$ is the photon energy, r is the radius of the photoelectron shell, and α is a calibration coefficient. A tunable laser with photon energy tuned slightly above the threshold was usually used to obtain high-resolution energy spectra. In the present experiment, a dye laser (Spectra-Physics) and an OPO laser (Spectra-Physics primoScan) were used. The dye laser pumped by a 532-nm Nd:YAG laser (Quanta-Ray Lab 190) had a narrow linewidth of $0.06\ cm^{-1}$. The photon energy ranged $11\,111$–$18\,484\ cm^{-1}$. The wavelength was monitored by a wavelength meter (HighFinesse WS6-600) with an
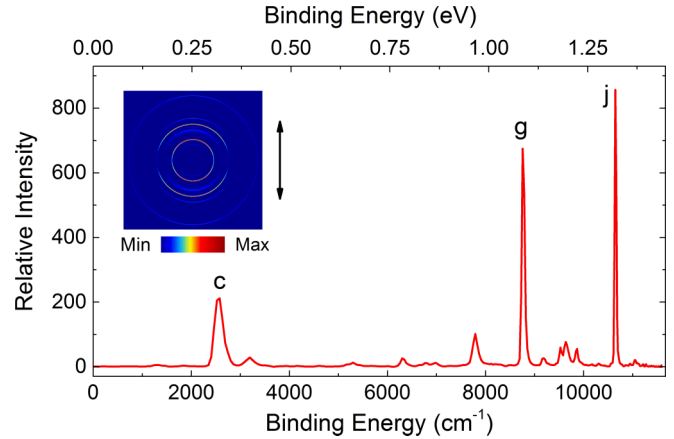

FIG. 2. Photoelectron image and spectrum of ions with $m = 238$ at photon energy $11\,590\ cm^{-1}$. The strong peaks c, g, and j are from U−. The double-headed arrow indicates the laser polarization.

accuracy of $0.02\ cm^{-1}$. The OPO laser was pumped by a 355-nm Nd:YAG laser (Quanta-Ray Lab 190). The wavelength ranged 400–2700 nm. The linewidth was about $5\ cm^{-1}$.

The target used in this experiment was a depleted uranium metal disk. With the laser ablation ion source, a strong UH− ($m = 239$) signal and a weak U− ($m = 238$) signal were observed in the mass spectra. Figure 2 shows a typical photoelectron imaging and energy spectrum of ions with $m = 238$. It was obtained with the cold ion trap at 15 K using a mixture of 80% He and 20% H_2 as the buffer gas. The ion trap time was 45 ms, and the photon energy ($h\nu$) of the photodetachment laser was $11\,590\ cm^{-1}$. Three strong peaks were observed in Fig. 2. The energy levels of neutral U atoms are known to high accuracy, giving a "fingerprint" in support of the state assignment. Peak c is assigned to the photodetachment channel from the ground state of U− ($5f^36d7s^27p\ {}^6M^e_{13/2}$) to the ground state of U ($5f^36d7s^2\ {}^5L_6$). The anisotropic parameter β of photoelectron angular distributions for peak c is 0.45(0.21). The β value is 1.78(0.08) for peak g, and 1.46(0.05) for peak j. It deviates from the expected 2 for photodetachment of a $7s$ electron, which might be due to the strong electron correlation effects [47]. To reliably assign the other weak peaks, we collected photoelectron energy spectra at a series of photon energies since SEVI has a higher energy resolution for electrons with lower kinetic energies. Figure 3(a) shows the results of piecing together photoelectron spectra at different photon energies for ions with $m = 238$ and $m = 239$. It can be seen that the spectra for $m = 238$ has a contamination from UH− ($m = 239$) because the intensity of UH− is much stronger than that of U−. Peaks that appear only in the spectrum with $m = 238$ are assigned to U− and labeled with letters a-q. Peaks c-q correspond to transitions from the ground state of U−, and peaks a and b are related to the transitions from excited states of U−.

To further assign peaks a and b, we adjusted the operating parameters of the ion trap. Since the mixed gas of He + H_2 quenched the excited states of U− quickly, the pure He gas was used instead to investigate the dynamics of peaks a and b. Figure 3(b) compares the photoelectron energy
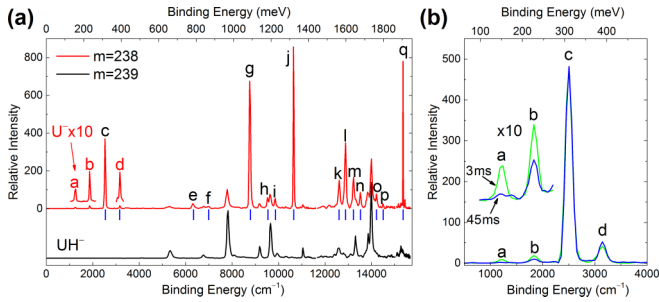
FIG. 3. (a) Photoelectron spectra of anions with $m = 238$ (red) and 239 (black). The spectrum with $m = 238$ includes signals of U$^-$ and UH$^-$ ions due to contaminations from the strong UH$^-$ signals, and the spectrum with $m = 239$ is contributed only by UH$^-$. Peaks a-q that appear only in the spectrum with $m = 238$ belong to U$^-$. The blue vertical spikes under the spectrum of U$^-$ indicate the energy levels of the neutral U atom. (b) Comparison of photoelectron spectra of U$^-$ when trap time is 3 ms (green) and 45 ms (blue). Peak intensities were normalized using peak c.

spectra when U$^-$ ions were stored in the trap for 3 and 45 ms. The spectra have been normalized to peak c. It can be seen that peak a decays much faster than peak b. Therefore, peaks a and b are related to two different excited states. According to the calculation of Beck and co-workers [30], we assigned peak a as $5f^36d7s^27p\ ^6L^e_{11/2} \rightarrow 5f^36d7s^2\ ^5L_6$, and $5f^36d^27s^2\ ^6M^o_{13/2} \rightarrow 5f^36d7s^2\ ^5L_6$ for peak b. By acquiring extra spectra with trap times equal to 6, 7, 8, 10, 15, 20, and 30 ms, the lifetimes of $5f^36d^27s^2\ ^6M^o_{13/2}$ and $5f^36d7s^27p\ ^6L^e_{11/2}$ were estimated to be 44 and 12 ms, respectively. According to Beck and co-workers' calculations [30], peak c is a result of detaching a p electron, while detaching a d electron for peak b. To verify this prediction, we measured the anisotropic parameter β of photoelectron angular distributions. As shown in Fig. 4, the trends of β are indeed different for peaks c and b as we tuned the photon energy from 4000 to 8000 cm^{-1}. To explain the results, we fitted the experimental data points using the simplified version of Cooper-Zare formula by Hanstorp *et al.* [47–50] for photodetaching a p electron and a d electron, respectively. Unfortunately, the simplified Cooper-Zare calculations cannot distinguish between photodetaching a p electron and
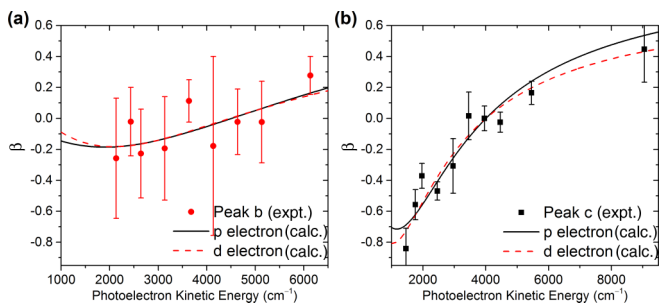

FIG. 4. The β values for the photoelectron angular distributions of peaks c and b. The dots are experimental results, and the solid and dashed lines were generated using the simplified version of Cooper-Zare formula by Hanstorp *et al.* for photodetaching a p electron and a d electron, respectively [47–50].
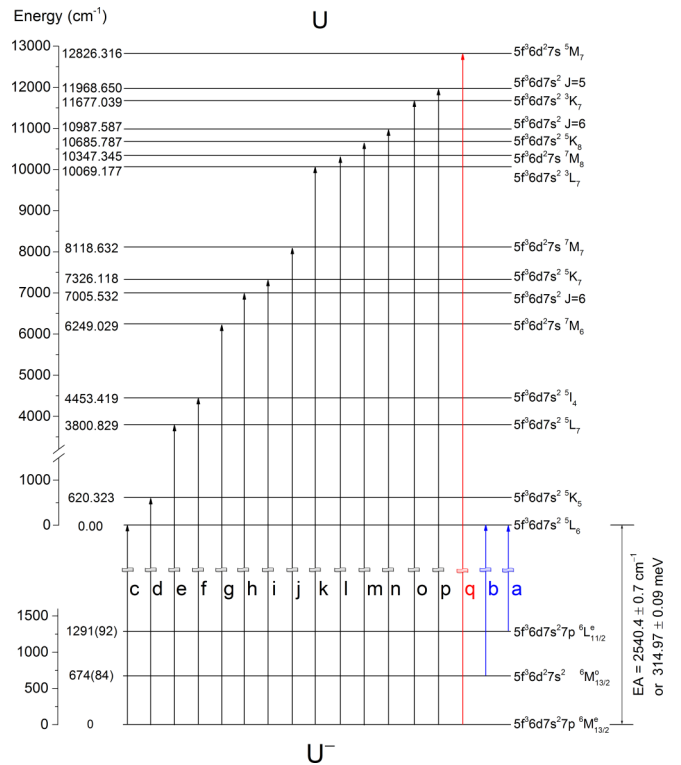

FIG. 5. Energy levels of U$^-$ and U related to the present measurement. The ground state of U is $5f^36d7s^2\ ^5L_6$. The ground state of U$^-$ is $5f^36d7s^27p\ ^6M_{13/2}$. The labels of each transition are consistent with the observed peaks in Figs. 2 and 3. The transition q is used for the electron affinity measurement.

a d electron in our situation due to two free parameters in the formula [47–50], hence we cannot unambiguously assign the ground state of U$^-$ as $^6M^e_{13/2}$ or $^6M^o_{13/2}$ based on the experimental results. High-level *ab initio* theories without adjustable parameters are required to solve this dilemma. We tentatively assigned the states according to the calculations by Beck and co-workers [30]. It should be pointed out that the measured lifetime of the first excited state is 44 ms, which is a typical value for an electric dipole ($E1$) transition. The lifetime for an electric quadrupole ($E2$) or magnetic dipole ($M1$) transition should be several orders of magnitude longer. As a reference, the lifetime for the first excited state in Th$^-$ (401 cm^{-1} above the ground state) is 51.3 ms due to an $E1$ transition [21]. Therefore, we believe that the parity between the first excited state and the ground state in U$^-$ is opposite, being consistent with the calculations by Beck and co-workers [30]. All observed transitions are illustrated in Fig. 5 and their binding energies are listed in Table I.

To determine the EA value of U as accurately as possible, we have chosen the strong peak q for the EA measurement since its binding energy lies in the tuning range of our dye laser. Five spectra were acquired with photon energies ranging 15 413–15 513 cm^{-1} with a step of 20 cm^{-1}, slightly above the threshold energy of q. We plot $h\nu$ vs r^2 in Fig. 6, where r is the radius of the photoelectron shell of transition q. Since $h\nu = \text{BE} + ar^2$, the intercept of the fitted line indicates the binding energy (BE) of transition q, which was determined to be 15 366.7(7) cm^{-1}. According to the NIST atomic database,

TABLE I. Measured binding energies and assigned binding energies of transitions observed in the present work.

Peak	Levels (U ← U⁻)	Measured binding energy (cm^{-1})	Assigned binding energy (cm^{-1}) [a]
a	$5f^36d7s^2\ ^5L_6 \leftarrow 5f^36d7s^27p\,^6L^e_{11/2}$	1249(92)	1249(92)
b	$5f^36d7s^2\ ^5L_6 \leftarrow 5f^36d7s^2\,^6M^o_{13/2}$	1866(84)	1866(84)
c	$5f^36d7s^2\ ^5L_6 \leftarrow 5f^36d7s^27p\,^6M^e_{13/2}$	2524(31)	2540.4(7)
d	$5f^36d7s^2\ ^5K_5 \leftarrow 5f^36d7s^27p\,^6M^e_{13/2}$	3181(43)	3160.7(7)
e	$5f^36d7s^2\ ^5L_7 \leftarrow 5f^36d7s^27p\,^6M^e_{13/2}$	6337(18)	6341.3(7)
f	$5f^36d7s^2\ ^5I_4 \leftarrow 5f^36d7s^27p\,^6M^e_{13/2}$	6991(17)	6993.8(7)
g	$5f^36d^27s\ ^7M_6 \leftarrow 5f^36d7s^27p\,^6M^e_{13/2}$	8786(10)	8789.5(7)
h	$5f^36d7s^2J = 6 \leftarrow 5f^36d7s^27p\,^6M^e_{13/2}$	9550(9)	9546.0(7)
i	$5f^36d7s^2\ ^5K_7 \leftarrow 5f^36d7s^27p\,^6M^e_{13/2}$	9866(7)	9866.5(7)
j	$5f^36d^27s\ ^7M_7 \leftarrow 5f^36d7s^27p\,^6M^e_{13/2}$	10 658(3)	10 659.1(7)
k	$5f^36d7s^2\ ^3L_7 \leftarrow 5f^36d7s^27p\,^6M^e_{13/2}$	12 609(3)	12 609.6(7)
l	$5f^36d^27s\ ^7M_8 \leftarrow 5f^36d7s^27p\,^6M^e_{13/2}$	12 887(3)	12 887.8(7)
m	$5f^36d7s^2\ ^5K_8 \leftarrow 5f^36d7s^27p\,^6M^e_{13/2}$	13 231(6)	13 226.2(7)
n	$5f^36d7s^2J = 6 \leftarrow 5f^36d7s^27p\,^6M^e_{13/2}$	13 526(3)	13 528.0(7)
o	$5f^36d7s^2\ ^3K_7 \leftarrow 5f^36d7s^27p\,^6M^e_{13/2}$	14 222(9)	14 217.5(7)
p	$5f^36d7s^2J = 5 \leftarrow 5f^36d7s^27p\,^6M^e_{13/2}$	14 499(12)	14 509.1(7)
q	$5f^36d^27s\ ^5M_7 \leftarrow 5f^36d7s^27p\,^6M^e_{13/2}$	15 366.7(7)	15 366.7(7)

[a]Deduced value according to the assignment, the measured EA value, the optimized binding energy of transitions measured in the present work, and the energy levels of neutral U [51].

the final state $5f^36d^27s\ ^5M_7$ is 12 826.316 cm^{-1} above the ground state [51]. The EA value of U was given by subtracting 12 826.316 cm^{-1} from 15 366.7(7) cm^{-1}. As a result, EA(U) was determined to be 2540.4(7) cm^{-1} or 314.97(9) meV. Note that $1\,\mathrm{eV} = 8065.543\,937$ cm^{-1}, as recommended by 2018 CODATA [52].
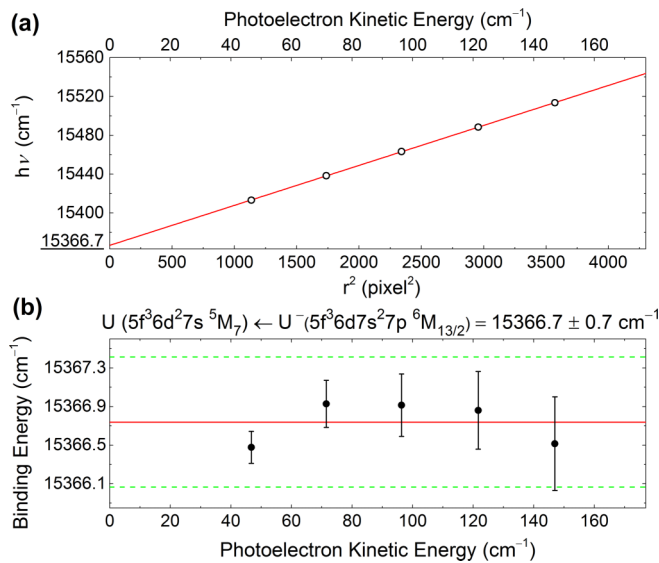

FIG. 6. (a) The photon energy $h\nu$ versus the squared radius r^2 of the photoelectron spherical shell for transition q ($5f^36d^27s\ ^5M_7 \leftarrow 5f^36d7s^27p\,^6M_{13/2}$). The solid line is the linear least-squares fitting. The intercept 15 366.7 cm^{-1} gives the binding energy of the photodetachment channel q. (b) The binding energy of transition q as a function of the kinetic energy of photoelectrons. The dashed lines indicate the uncertainty of ± 0.7 cm^{-1}.

The energy levels of the two excited states $5f^36d^27s^2\ ^6M^o_{13/2}$ and $5f^36d7s^27p\,^6L^e_{11/2}$ were extracted from the binding energy differences among transitions a, b, and c as they were from different initial states to the same final state. The binding energy of transition c is the EA value, while binding energies of transitions a and b were deduced by $\mathrm{BE} = h\nu - ar^2$, where the coefficient α was determined using the well-known transitions c, d, e, and g. Finally, the two excited $5f^36d^27s^2\ ^6M^o_{13/2}$ and $5f^36d7s^27p\,^6L^e_{11/2}$ were determined to be 674(84) cm^{-1} or 84(11) meV, and 1291(92) cm^{-1} or 160(12) meV above the ground state $5f^36d7s^27p\,^6M^e_{13/2}$, respectively. Our experimental results are in good agreement with the predictions by Beck's group in 2009 [30]. Experimental and calculated results are compared in Table II.

It should be pointed out that the transitions $5f^36d^27s^2\ ^6M^o_{13/2} \leftrightarrow 5f^36d7s^27p\,^6M^e_{13/2}$ and $5f^36d7s^27p\,^6L^e_{11/2} \leftrightarrow 5f^36d^27s^2\ ^6M^o_{13/2}$ are $E1$ allowed transitions. The transition $^6M^o_{13/2} \leftrightarrow {}^6M^e_{13/2}$ is perfectly closed because it is between the first excited state and the ground state and the nuclear spin of ^{238}U is zero. However,

TABLE II. The energy levels of bound states in U$^-$ and the electron affinity of U (meV).

State	O'Malley et al. (calculated) [30]	This work (measured)
$5f^36d7s^27p\ ^6M^e_{13/2}$	0	0
$5f^36d^27s^2\ ^6M^o_{13/2}$	113	84(11)
$5f^36d7s^27p\ ^6L^e_{11/2}$	182	160(12)
Electron affinity of U	373	314.97(9)

the transition energy is only 84(11) meV, which makes the cycling very slow because the transition rate is proportional to ν^3, and $\nu = 20(2)$ THz. The measured lifetime 44 ms of $^6M^o_{13/2}$ has verified this point. The advantage of this transition is that there is no photodetachment loss during laser cooling because the excitation energy to $^6M^o_{13/2}$ is less than EA(U)/2. The excited state $^6M^o_{13/2}$ cannot be photodetached by the second photon. The wavelength of the cooling transition $^6M^o_{13/2} \leftrightarrow {}^6M^e_{13/2}$ is 15 μm, which is in the range covered by the commercial quantum cascade laser. So far, no negative ions have been directly laser cooled because a cycling E1 transition is very rare in atomic anions. The present work provided convincing evidence that U$^-$ has a perfectly closed E1 transition between bound states. It should be pointed out that laser cooling of U$^-$ will be very challenging due to the slow cooling rate and the inevitable collision heating. It needs to scatter 2×10^5 photons to cool U$^-$ from 5 K to the temperature of Doppler limit. This will take 1.8×10^4 s if in saturation.

In conclusion, we have obtained the high-resolution photoelectron energy spectra of U$^-$ using the SEVI method. The electron affinity of U was measured to be 2540.4(7) cm^{-1} or 314.97(9) meV. Two excited states of U$^-$ were determined to be 674(84) cm^{-1} or 84(11) meV, and 1291(92) cm^{-1} or 160(12) meV above the ground state, respectively. The transition between the first excited state and the ground state of U$^-$ is an E1 allowed transition. Our experiments represent a different level of studying heavy atomic anions and can serve as a benchmark for developing different theoretical models.

[1] L. Gagliardi, M. C. Heaven, J. W. Krogh, and B. O. Roos, J. Am. Chem. Soc. **127**, 86 (2005).

[2] J. Han, L. A. Kaledin, V. Goncharov, A. V. Komissarov, and M. C. Heaven, J. Am. Chem. Soc. **125**, 7176 (2003).

[3] W.-L. Li, J. Su, T. Jian, G. V. Lopez, H.-S. Hu, G.-J. Cao, J. Li, and L. S. Wang, J. Chem. Phys. **140**, 094306 (2014).

[4] J. Czekner, G. V. Lopez, and L. S. Wang, J. Chem. Phys. **141**, 244302 (2014).

[5] J. Han, V. Goncharov, L. A. Kaledin, A. V. Komissarov, and M. C. Heaven, J. Chem. Phys. **120**, 5155 (2004).

[6] D. R. Beck, S. M. O'Malley, and L. Pan, *Computational Methods in Lanthanide and Actinide Chemistry* (Wiley, Chichester, UK, 2015).

[7] D. Leimbach, J. Karls, Y. Guo, R. Ahmed, J. Ballof, L. Bengtsson, F. B. Pamies, A. Borschevsky, K. Chrysalidis, E. Eliav, D. Fedorov, V. Fedosseev, O. Forstner, N. Galland, R. F. G. Ruiz, C. Granados, R. Heinke, K. Johnston, A. Koszorus, U. Köster *et al.*, Nat Commun. **11**, 3824 (2020).

[8] T. K. Sato, M. Asai, A. Borschevsky, T. Stora, N. Sato, Y. Kaneya, K. Tsukada, C. E. Düllmann, K. Eberhardt, E. Eliav, S. Ichikawa, U. Kaldor, J. V. Kratz, S. Miyashita, Y. Nagame, K. Ooe, A. Osa, D. Renisch, J. Runke, M. Schädel *et al.*, Nature (London) **520**, 209 (2015).

[9] K. Kozioł and G. A. Aucar, J. Chem. Phys. **148**, 134101 (2018).

[10] ACME Collaboration, Nature (London) **562**, 355 (2018).

[11] M.-A. Bouchiat and C. Bouchiat, Rep. Prog. Phys. **60**, 1351 (1999).

[12] P. Jerabek, B. Schuetrumpf, P. Schwerdtfeger, and W. Nazarewicz, Phys. Rev. Lett. **120**, 053001(2018).

[13] T. H. Dinh, V. A. Dzuba, V. V. Flambaum, and J. S. M. Ginges, Phys. Rev. A **78**, 022507 (2008).

[14] I. I. Tupitsyn, M. G. Kozlov, M. S. Safronova, V. M. Shabaev, and V. A. Dzuba, Phys. Rev. Lett. **117**, 253001 (2016).

[15] C. Hock, J. B. Kim, M. L. Weichman, T. I. Yacovitch, and D. M. Neumark, J. Chem. Phys. **137**, 244201 (2012).

[16] X. B. Wang and L. S. Wang, Rev. Sci. Instrum. **79**, 073108 (2008).

[17] R. L. Tang, X. X. Fu, and C. G. Ning, J. Chem. Phys. **149**, 134304 (2018).

[18] R. L. Tang, X. X. Fu, Y. Lu, and C. G. Ning, J. Chem. Phys. **152**, 114303 (2020).

[19] X. X. Fu, R. L. Tang, Y.-Z. Lu, and C. G. Ning, Chin. J. Chem. Phys. **32**, 187 (2019).

[20] Y. Lu, R. L. Tang, X. X. Fu, and C. G. Ning, Phys. Rev. A **99**, 062507 (2019).

[21] R. Tang, R. Si, Z. Fei, X. Fu, Y. Lu, T. Brage, H. Liu, C. Chen, and C. Ning, Phys. Rev. Lett. **123**, 203002 (2019).

[22] X. Fu, Y. Lu, R. Tang, and C. Ning, Phys. Rev. A **101**, 022502 (2020).

[23] Z. Luo, X. Chen, J. Li, and C. Ning, Phys. Rev. A **93**, 020501(R) (2016).

[24] X. L. Chen and C. G. Ning, J. Phys. Chem. Lett. **8**, 2735 (2017).

[25] R. L. Tang, X. L. Chen, X. X. Fu, H. Wang, and C. G. Ning, Phys. Rev. A **98**, 020501(R) (2018).

[26] H. Hotop and W. C. Lineberger, J. Phys. Chem. Ref. Data **14**, 731 (1985).

[27] D. M. Neumark, K. R. Lykke, T. Andersen, and W. C. Lineberger, Phys. Rev. A **32**, 1890 (1985).

[28] M.-J. Nadeau, M. A. Garwan, X.-L. Zhao, and A. E. Litherland, Nucl. Instrum. Methods Phys. Res., Sect. B **123**, 521 (1997).

[29] J. Emsley, *Nature's Building Blocks: An AZ Guide to the Elements* (Oxford University Press, Oxford, UK, 2011).

[30] S. M. O'Malley and D. R. Beck, Phys. Rev. A **80**, 032514 (2009).

[31] R. C. Bilodeau and H. K. Haugen, Phys. Rev. Lett. **85**, 534 (2000).

[32] A. Kellerbauer and J. Walz, New J. Phys. **8**, 45 (2006).

[33] U. Warring, M. Amoretti, C. Canali, A. Fischer, R. Heyne, J. O. Meier, C. Morhard, and A. Kellerbauer, Phys. Rev. Lett. **102**, 043001 (2009).

[34] A. Fischer, C. Canali, U. Warring, A. Kellerbauer, and S. Fritzsche, Phys. Rev. Lett. **104**, 073004 (2010).

[35] L. Pan and D. R. Beck, Phys. Rev. A **82**, 014501 (2010).

[36] C. W. Walter, N. D. Gibson, D. J. Matyas, C. Crocker, K. A. Dungan, B. R. Matola, and J. Rohlen, Phys. Rev. Lett. **113**, 063001 (2014).

[37] E. Jordan, G. Cerchiari, S. Fritzsche, and A. Kellerbauer, Phys. Rev. Lett. **115**, 113001 (2015).

[38] G. Cerchiari, A. Kellerbauer, M. S. Safronova, U. I. Safronova, and P. Yzombard, Phys. Rev. Lett. **120**, 133205 (2018).

[39] C. W. Walter, N. D. Gibson, C. M. Janczak, K. A. Starr, A. P. Snedden, R. L. Field, III, and P. Andersson, Phys. Rev. A **76**, 052702 (2007).

[40] C. W. Walter, N. D. Gibson, Y. G. Li, D. J. Matyas, R. M. Alton, S. E. Lou, R. L. Field, D. Hanstorp, L. Pan, and D. R. Beck, Phys. Rev. A **84**, 032514 (2011).

[41] R. L. Tang, R. Si, Z. J. Fei, X. X. Fu, Y. Z. Lu, T. Brage, H. T. Liu, C. Y. Chen, and C. G. Ning, Phys. Rev. A **103**, 042817 (2021).

[42] K. D. Dinov and D. R. Beck, Phys. Rev. A **52**, 2632 (1995).

[43] J. B. Kim, M. L. Weichman, and D. M. Neumark, Mol. Phys. **113**, 2105 (2014).

[44] W. C. Wiley and I. H. McLaren, Rev. Sci. Instrum. **26**, 1150 (1955).

[45] I. León, Z. Yang, H. T. Liu, and L. S. Wang, Rev. Sci. Instrum. **85**, 083106 (2014).

[46] B. Dick, Phys. Chem. Chem. Phys. **16**, 570 (2014).

[47] Y. Lu, J. Zhao, R. L. Tang, X. X. Fu, and C. G. Ning, J. Chem. Phys. **152**, 034302 (2020).

[48] J. Cooper and R. N. Zare, J. Chem. Phys. **49**, 4252 (1968).

[49] J. Cooper and R. N. Zare, J. Chem. Phys. **48**, 942 (1968).

[50] D. Hanstorp, C. Bengtsson, and D. J. Larson, Phys. Rev. A **40**, 670 (1989).

[51] J. E. Sansonetti and W. C. Martin, J. Phys. Chem. Ref. Data **34**, 1559 (2005).

[52] E. Tiesinga, P. J. Mohr, D. B. Newell, and B. N. Taylor, 2018 NIST CODATA recommended values of the fundamental physical constants (NIST, Gaithersburg, MD), http://physics.nist.gov/constants (retrieved 2019).